Shape Entropy of a Reconfigurable Ising Surface

Benjamin N. Katz,* Lev Krainov,† and Vincent Crespi‡
Department of Physics, The Pennsylvania State University, 104 Davey Lab, University Park, Pennsylvania 16802, USA

(Received 3 September 2021; revised 24 March 2022; accepted 16 July 2022; published 26 August 2022)

Disclinations in a 2D sheet create regions of Gaussian curvature whose inversion produces a reconfigurable surface with many distinct metastable shapes, as shown by molecular dynamics of a disclinated graphene monolayer. This material has a near-Gaussian "density of shapes" and an effectively antiferromagnetic interaction between adjacent cones. A ~ 10 nm patch has hundreds of distinct metastable shapes with tunable stability and topography on the size scale of biomolecules. As every conical disclination provides an Ising-like degree of freedom, we call this technique "Isigami."

DOI: 10.1103/PhysRevLett.129.096102

Techniques arising from papercraft—origami and kirigami—inspire efforts to impart three-dimensional shapes to two-dimensional materials [1–13]. Origami and kirigami both work by imposing *one*-dimensional modifications (folds or cuts) into surfaces. Here we investigate an alternative method of shape control that inserts *zero*-dimensional objects—isolated disclinations—into an atomically thin sheet. Inversion of bistable conical disclinations provides a means to control the shape of the surface, with tunable topography down to the length scale of protein secondary or tertiary structure and energy barriers against shape change that are tunable from below room temperature to values much larger. A tunable topography in a biologically relevant size regime suggests that reconfigurable shape-driven binding interactions may be possible with such sheets.

A disclination removes or adds a wedge of material in the lattice of a two-dimensional sheet, yielding a conical or hyperbolic local region; in a hexagonal lattice, the least costly such defects are five- and seven-membered rings. Since a cone (in a continuum approximation) has a local C_∞ symmetry for rotations about its apex, its mechanical states are anticipated to be particularly simple: just "up" and "down," related by a local inversion. The reduced rotational symmetry of the saddle suggests more complex behavior, as it may be able to assume more than one in-plane orientation depending on the local mechanical environment. Here we investigate a sheet containing multiple disclinations balanced between positive and negative (i.e., asymptotically flat) and determine the multiplicity and character of the shape metastability thereby instilled in the 2D layer. Anticipating our conclusions, the sheet's conformational freedom is dominated by Ising-like bistable cone degrees of freedom; hence we call this means of shape control Isigami.

To create such a surface, we begin with a so-called Haeckelite [14,15] structure and "inflate" each ring with a penumbra of hexagons, similar to inflation of larger fullerenes from C_{60} [16,17]. We choose a Haeckelite in which the pentagonal rings form a slightly deformed kagome lattice (Fig. 1) [18]. The shape entropy phenomena that we seek to study should not require an ordered lattice of disclinations; this choice is for computational convenience and to explore whether ideal mechanical frustration may bring the set of possible shapes closer to mutual degeneracy. Other disclination patterns are also possible, and those formed by phase field crystal methods have been examined independently for their effect on sheet toughness in work by Zhang *et al.* [19]. We choose graphene as an archetype, since its mechanical response is well studied and methods exist to functionalize the surface to control mechanical stiffness, interfacial energetics, and hydrophilicity [20–22]. Since the behavior described below is largely geometrical in origin, conclusions derived from graphene Isigami should generalize to other atomically thin two-dimensional materials.

We construct both periodic- and finite-patch regions of material hosting 12 cones and 12 saddles on a kagome lattice as depicted in Fig. 1 and model the mechanical response using the adaptive intermolecular reactive empirical bond order (AIREBO) potential [23] as implemented in LAMMPS [24,25], as it is well validated for the mechanical response of nanoscale sp^2 carbon [26–30]. We first examine a finite sheet whose disclinations are separated by six hexagons ($\sim$20 Å); the edges are terminated by hydrogen. This separation is large enough that even cones on the edge of the sheet have two well-defined metastable up and down orientations. Shape variation is most dramatic in a finite patch of material, as the periodic boundary constraint is absent. The patch is systematically forced into every possible set of cone orientations by mechanically inverting various sets of cones. To this end, a force of ± 1.7 eV/Å is applied to the five atoms at the apices of various cones according to the desired up and down states, and the system is then allowed to evolve for 500 fs, while the atoms are constrained to move no more than 0.1 Å each time step. A constraint force is also applied evenly across every atom

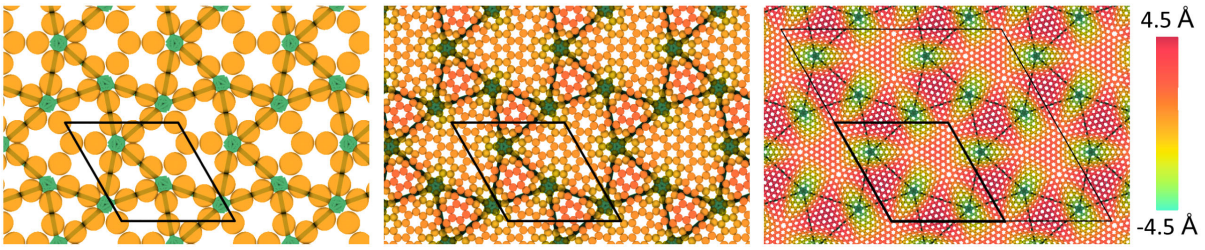

FIG. 1. Three versions of a graphene-based Isigami sheet with different disclination spacings. The first, with adjoining defects, is a Haeckelite known from [14]. The second and third have two- and six-hexagon wide buffers between pairs of disclinations. Sheets are color coded by height, whose variation grows for wider buffers (the first sheet being perfectly flat). Blue lines delineate a twisted kagome lattice of pentagonal disclinations. The larger unit cell marked on the third sheet shows the size of the system most closely studied (in either periodic or finite-patch geometries), containing 12 pentagonal and 12 heptagonal disclinations.

in the system to zero out the net force. The structure is then relaxed, either through a thermal bath at 300 K for 50 ps, followed by a linear ramp anneal over 30 ps from 300 to 3 K, or (for the periodic systems described below) through a shorter 1 ps thermal bath followed by a series of conjugate gradient minimizations where the unit cell geometry is allowed to relax during alternate optimization steps. These methods both produce well-converged energy minima (converged to less than 100 meV in systems with thousands of atoms), but the anneal method performs better for the finite patch in avoiding local minima.

For every initial choice of the 12 up or down cone configurations, the system relaxes into a distinct metastable shape, i.e., all 2^{12} nominal Isigami configurations are accessible. Figure 2 shows some examples of these shapes,

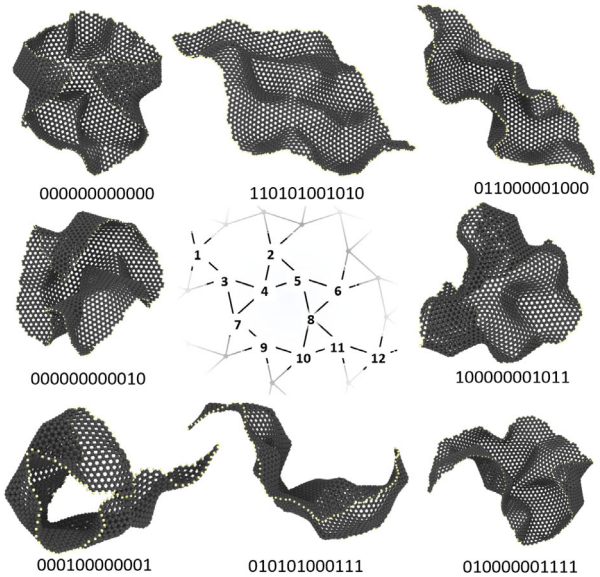

FIG. 2. Representative shapes for a 12-cone patch, as a demonstration of the multiplicity of metastable shapes. The shapes are displayed in their minimum energy states and are hydrogen terminated (yellow atoms) with carbon atoms in gray. A bit string of cone states in the sheet is displayed below each example; this labeling follows the order shown at center.

labeled by the cone configuration: the different shapes that are metastably assumed by the same sheet can be dramatically different. Several of these configurations, including the five highest in energy, were simulated at 800 K in an *NPT* ensemble for one nanosecond, with the sheet maintaining its original Ising state. This high-temperature "challenge" anneal was also applied to a subset of configurations that were repeated to create a 2×2 supercell patch, providing assurance that shape metastability is preserved for larger patch sizes as well.

Collapsing the reflection symmetry about the sheet midplane, we actually obtain 2^{11} distinct Isigami configurations for this 12-pentagon patch, with an additional approximate reflection symmetry about the short diagonal (broken very weakly by the detailed termination of the patch). Additional symmetries in the periodic case further reduce the number of symmetry-distinct configurations per unit area, but the conformational entropy of metastable Isigami states remains extensive.

As noted earlier, whereas cones have two distinct conformations (i.e., up and down), the metastable orientations of the principal axes of saddle-point disclinations are not naturally twofold; their number depends on their surroundings. We do in fact find certain conformations that have the same set of cone orientations (i.e., the same Isigami state) but visibly different overall shapes, sometimes differing by over an eV in energy and stable in shape up to at least 800 K over half a nanosecond. Figure 3 depicts two such states. While we have not exhaustively quantified the frequency of these non-Ising states, our observations suggest they contribute a number of configurations equivalent to roughly one additional Ising degree of freedom for a 12-cone sheet; i.e., their contribution to the overall configurational entropy is modest. Although these non-Ising states do sometimes correspond to different orientations of the saddle disclinations, we do not find a simple rule governing their appearance, as reflected by the examples shown in Fig. S5 [31]. Similar non-Ising states are seen in the larger 2×2 supercell patch. Simulations of this larger patch (and larger periodic systems) reveal a similarly pervasive metastability to Ising conformations,

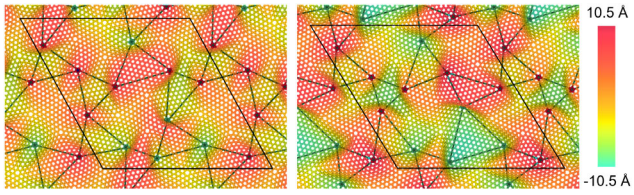

FIG. 3. Two periodic states with the same cone orientations but different metastable shapes: the state on the right is 6.5 eV lower in energy. The images are color coded by height on the same scale, and the deformed kagome lattice of each is shown in blue. Cones pointing up have red apices; those pointing down are blue.

suggesting that the system has an extensive conformational shape entropy.

How are these states distributed in energy? The density of shapes (i.e., the number of shapes in a given energy range) for the finite 12-cone patch is strikingly close to Gaussian, as shown in Fig. 4. It is tempting to consider this outcome as an expression of the central limit theorem for multiple nearly independent energetic contributions from different disclinations, but the stronger deviations from a Gaussian shape seen in a similarly sized periodic patch argue against a simple application of this notion. The distribution for the finite patch may be more Gaussian because its boundary condition produces multiple symmetry-distinct pentagonal disclinations within the patch and these heterogeneous local environments, under the action of elastic interactions that span the entire patch, yield something closer to the requirements of the central limit theorem. In contrast, every pentagonal disclination under periodic boundary conditions is symmetry equivalent. For less well-ordered disclination networks, we anticipate the periodic case to more closely approach the finite-patch distribution.

Mechanical intuition suggests that nearby cones will have pairwise antiferromagnetic interactions, since opposing up and down orientations produce compatible sidewall slopes. In practice, we find that longer-range and many-body elastic interactions between disclinations are too strong to admit a strict frustration-derived degeneracy. While these nonidealities (and also non-Isigami states) are sufficiently important that the sheet is not a simple nearest-neighbor antiferromagnet, the energies of different sheet configurations *do* reveal an overall nearest-neighbor antiferromagnetic trend, as the energy varies systematically with the number of oppositely oriented nearest-neighbor cones for both the periodic-boundary and finite-patch cases (Fig. 5). The effective J of this trend is proportionately smaller for a sheet with one-hexagon separation between the fivefold rings (Fig. S1 [31]). As noted in the Supplemental Material [31], it was not possible to describe the sheet energetics with a simple cluster expansion [32]; this was likely due in part to the long-range nature of elastic interactions among nearby cones (i.e., when even a single cone inverts, we see significant changes in shape across the entire patch, as shown in Fig. S4) and in part to the presence of a modest number of additional states not fully specifiable by an Isigami state vector, as noted earlier.

These reconfigurable surfaces provide a means to access a multitude of distinct sheet topographies from a single patch of multiply disclinated 2D material: an obvious area of potential application for such an object is shape recognition and binding of biomolecules. Ideally, such a surface would have topography on the length scale of

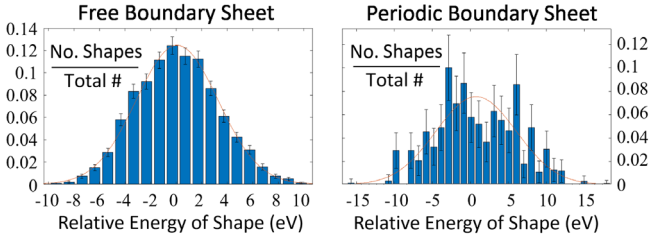

FIG. 4. The number of shapes of the 12-cone patches studied versus their relaxed energy, as a fraction of the total number of shapes examined for both finite and periodic sheets, with a normal distribution superimposed. The error bars follow $\sqrt{N}$.

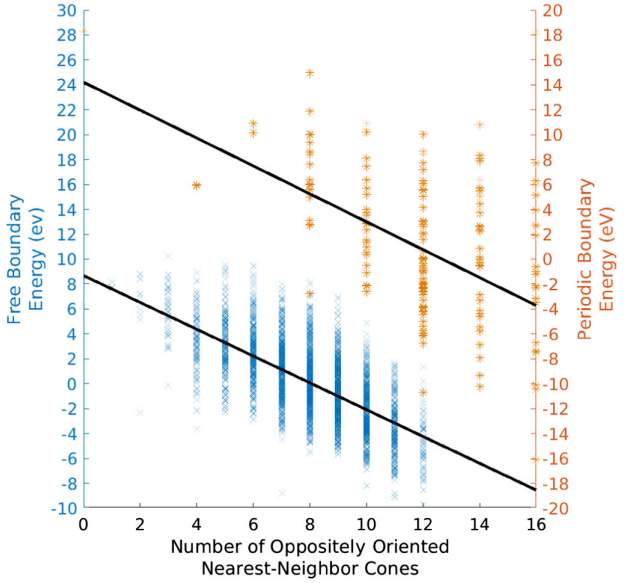

FIG. 5. The sheet energy as a function of the number of nearest-neighbor cone pairs that are oppositely oriented for both free (left, blue) and periodic (right, orange) boundary conditions, with least-squares linear fits. A nearest-neighbor pairwise antiferromagnetic interaction between pentagonal disclinations would yield a linear dependence, buried under significant variation from longer-ranged interactions, boundary effects, and a modest admixture of non-Ising states, as seen. The linear trend yields similar nearest-neighbor antiferromagnetic J's for free (-0.54 eV) and periodic (-0.56 eV) cases. The free-boundary case has fewer degeneracies and hence more distinct points. Points are translucent to better reveal the overall density of configurations.

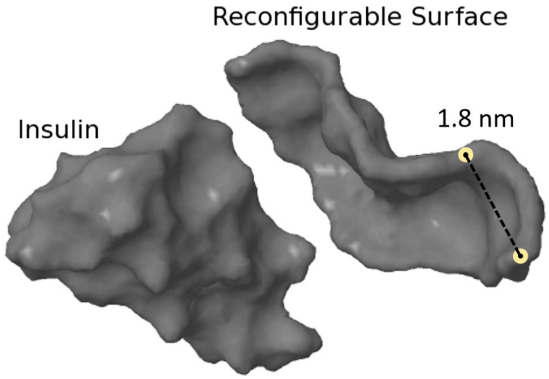

FIG. 6. Comparison between an Isigami sheet (at right) with a two-hexagon buffer between cones and a generic small protein (insulin, at left) that has been smoothed using the Connolly ("rolling ball") method for constructing solvent-excluded surfaces, done here with a solvent radius similar to the bending radius of the sheet to accentuate the topography of both across the same length scale, showing it is possible to construct Isigami sheets with reconfigurable topography on the same length scale as a protein's secondary or tertiary structure.

protein tertiary structure, a hydrophilic surface that does not denature biomolecules, and a tunable barrier against shape change so that both dynamic ($\sim k_B T$) and static ($\gg k_B T$) regimes can be accessed. The $\sim$0.5 nm interpentagon spacing of the sheet depicted in Fig. 6 provides topography on a biologically relevant length scale, as demonstrated by the comparison to insulin, a small protein, in the same figure. The use of graphene *oxide* [33,34] rather than hydrophobic bare graphene [35–37] could introduce the needed hydrophilicity and perhaps also increased flexibility [38].

The question of barrier height control requires more detailed study. The inversion barriers of isolated graphene cones have been simulated previously [39]; the barrier depends on the chemical character of the conical apex but is generally multiple electron volts for well-separated cones. Energy barriers against cone inversion will depend on the material of the sheet, the separation between conical disclinations, functionalization [39], or grain boundaries interconnecting disclinations [40,41]. We observe in the periodic sheets that the stability of the Ising and non-Ising states indeed varies with cone separation, and also that the barriers against interconversion of the non-Ising states are typically much lower than those between Ising configurations. We monitored the energy during cone inversion for a few periodic sheets with different cone separations; although the distribution of inversion barriers could not be exhaustively quantified, the barriers all remained on the order of electron volts, likely lowered somewhat (compared to isolated cones) by irregularities in the local environment. The typical barrier height scales roughly linearly with the separation between pentagonal disclinations, being around 1 eV for a one-hexagon separation and around 6 eV for the six-hexagon separation. At the one-hexagon separation, a significant fraction of the Isigami states destabilize (see Fig. S2 [31]), while almost all of the non-Ising states disappear, where our criterion for stability is surviving the room-temperature anneal mentioned earlier.

Since most of the cases considered above have inversion barriers much greater than $k_B T$, we now consider a means to "thermalize" these barriers even at larger disclination separations: oxidizing the sheet and etching away the central five-membered ring and one or more surrounding rings to reduce the mechanical deformation associated with nucleating inversion, terminating the resulting apical multivacancy with hydrogen atoms. To this end, we oxidized a six-hexagon-separation periodic sheet by random placement of oxygen atoms equally onto upper and lower surfaces, followed by a structural relaxation and subsequent removal of any unreacted oxygen, yielding a functionalized sheet with 12.6 at.% oxygen (Fig. S3 [31]). The apices of this sheet up to three surrounding rings were etched away by manual deletion, and the resulting edges were terminated with hydrogen. These simulations used a version of the REAXFF reactive force field [42–44] designed [45] to describe carbon, hydrogen, and oxygen [46] and updated to more precisely describe chemical properties of C/H/O/N systems [47–50]. Neither the structural relaxation following etching (nor that which followed oxygenation) caused cone inversion, but during a subsequent MD simulation at 800 K we observe rapid ($\sim$1 ns) spontaneous inversion of cones; we expect a similar simulation without periodic boundary conditions to be at least as floppy. Although these simulations were performed in the gas phase, we anticipate that the qualitative conclusion of low, thermally accessible inversion barriers will be robust against the introduction of aqueous conditions (which may themselves further reduce the barrier). In contrast, the same system with unetched apices shows no inversion over 1 ns at 800 K.

Shape reconfigurability at the nanometer-to-micron scale is a signature of biology, but one that is not straightforwardly expressed in nonbiological systems. We describe a strategy toward this end that uses the bistability of disclinations to afford a large library of shapes from a single 2D sheet. Selection from this library could either happen spontaneously—for example, through binding interactions with targets under conditions of shape lability—or be imposed through mechanical deformation by a specified indenter. We demonstrate the second of these through large-scale molecular dynamics simulations of indented Isigami sheets. The simulated sheets are large enough to be compatible with experimental nano- or micromechanical manipulation [51,52] (i.e., hundreds of nanometers across) and make use of simple radial and annular indenter geometries, as depicted in the Supplemental Material [31], Videos S1–S3. The three sheets simulated all start from the same asymptotically flat Ising configuration. The indenters' pressures force all the cones underneath to orient similarly, which creates linear structures of unbalanced (i.e., ferromagnetically aligned) Ising state. The antiferromagnetic interaction

between neighboring cones in the indented region then drives a sheet distortion that splays these cones away from each other to minimize their unfavorable coalignment: the resulting crumples "bunch up" material under the indented region. For the radial indenter, this bunching reduces the circumference at fixed radius from the center of the indenter, while the annular indenter does the opposite; thus they create large-scale Gaussian curvatures of opposite sign. The cross-shaped indenters of different widths also produce different bend angles. We apply fourfold symmetric indenters to show that vertices defined by the intersection of four folds can be easily created, while a generic crumpled fold would involve only three. These deformations should be reversible by compressing between flat planes and reindenting.

As this approach is purely geometrical, it should apply to any atomically thin sheet, which could be polar (*h*-BN), hydrophilic (graphene oxide [33,34]), or stiffer than graphene [53]. These phenomena should also occur in more irregular disclination networks that could be produced by, e.g., growing a 2D layer on a roughened substrate, as strict degeneracies due to mechanical frustration on a regular lattice were neither observed nor required: mechanical bistability is a local property of each conical disclination, one whose antiferromagnetic near-neighbor interactions then favor a large shape multiplicity. The degree of metastability is tunable from highly stable to potentially room-temperature reconfigurable. Possible longer-term applications for 2D shape reconfiguration could involve diverse shape libraries exposed to binding targets under shape-labile conditions, selected for binding, and then utilized under shape-conserving conditions. On longer length scales, linear arrays of disclinations could recover phenomena akin to more traditional fold-based origami wherein mean curvature plays a more prominent role. The presence of disclinations (with associated geometrical phases [54]) and local strains (with associated pseudomagnetic fields [55–58]) may also introduce unusual electronic and plasmonic [59] properties.

B. N. K. acknowledges training provided by the Computational Materials Education and Training (CoMET) NSF Research Traineeship (Grant No. DGE-1449785). B. N. K., L. K., and V. H. C. acknowledge support under NSF Grants No. DMR-2011839 and No. DMR-2039351. Many thanks to Dr. Malgorzata Kowalik for her assistance with ADF and ReaxFF potentials.

*bnk120@psu.edu
†lxk67@psu.edu
‡vhc2@psu.edu

[1] M. K. Blees, A. W. Barnard, P. A. Rose, S. P. Roberts, K. L. McGill, P. Y. Huang, A. R. Ruyack, J. W. Kevek, B. Kobrin, D. A. Muller, and P. L. McEuen, Graphene kirigami, Nature (London) **524**, 204 (2015).
[2] S. J. Callens and A. A. Zadpoor, From flat sheets to curved geometries: Origami and kirigami approaches, Mater. Today **21**, 241 (2018).
[3] J.-H. Cho, M. D. Keung, N. Verellen, L. Lagae, V. V. Moshchalkov, P. V. Dorpe, and D. H. Gracias, Nanoscale origami for 3d optics, Small **7**, 1943 (2011).
[4] H. Dietz, S. M. Douglas, and W. M. Shih, Folding DNA into twisted and curved nanoscale shapes, Science **325**, 725 (2009).
[5] D. Han, X. Qi, C. Myhrvold, B. Wang, M. Dai, S. Jiang, M. Bates, Y. Liu, B. An, F. Zhang, H. Yan, and P. Yin, Single-stranded DNA and RNA origami, Science **358**, eaao2648 (2017).
[6] P. Z. Hanakata, Z. Qi, D. K. Campbell, and H. S. Park, Highly stretchable MoS2 kirigami, Nanoscale **8**, 458 (2016).
[7] Y. Morikawa, S. Yamagiwa, H. Sawahata, R. Numano, K. Koida, M. Ishida, and T. Kawano, Ultrastretchable kirigami bioprobes, Adv. Healthcare Mater. **7**, 1701100 (2018).
[8] B. Mortazavi, A. Lherbier, Z. Fan, A. Harju, T. Rabczuk, and J.-C. Charlier, Thermal and electronic transport characteristics of highly stretchable graphene kirigami, Nanoscale **9**, 16329 (2017).
[9] L. Xu, X. Wang, Y. Kim, T. C. Shyu, J. Lyu, and N. A. Kotov, Kirigami nanocomposites as wide-angle diffraction gratings, ACS Nano **10**, 6156 (2016).
[10] L. Xu, T. C. Shyu, and N. A. Kotov, Origami and kirigami nanocomposites, ACS Nano **11**, 7587 (2017).
[11] Y. Zhang *et al.*, A mechanically driven form of kirigami as a route to 3D mesostructures in micro/nanomembranes, Proc. Natl. Acad. Sci. U.S.A. **112**, 11757 (2015).
[12] D. Akinwande *et al.*, A review on mechanics and mechanical properties of 2D materials—Graphene and beyond, Extreme Mech. Lett. **13**, 42 (2017).
[13] Y. Wei and R. Yang, Nanomechanics of graphene, Natl. Sci. Rev. **6**, 324 (2019).
[14] H. Terrones, M. Terrones, E. Hernández, N. Grobert, J.-C. Charlier, and P. M. Ajayan, New Metallic Allotropes of Planar and Tubular Carbon, Phys. Rev. Lett. **84**, 1716 (2000).
[15] V. H. Crespi, L. X. Benedict, M. L. Cohen, and S. G. Louie, Prediction of a pure-carbon planar covalent metal, Phys. Rev. B **53**, R13303 (1996).
[16] P. W. Dunk, N. K. Kaiser, C. L. Hendrickson, J. P. Quinn, C. P. Ewels, Y. Nakanishi, Y. Sasaki, H. Shinohara, A. G. Marshall, and H. W. Kroto, Closed network growth of fullerenes, Nat. Commun. **3**, 855 (2012).
[17] T. Suzuki, Q. Li, K. C. Khemani, F. Wudl, and O. Almarsson, Systematic inflation of buckminsterfullerene C_{60}: Synthesis of diphenyl fulleroids C_{61} to C_{66}, Science **254**, 1186 (1991).
[18] K. Sun, A. Souslov, X. Mao, and T. C. Lubensky, Surface phonons, elastic response, and conformal invariance in twisted kagome lattices, Proc. Natl. Acad. Sci. U.S.A. **109**, 12369 (2012).
[19] T. Zhang, X. Li, and H. Gao, Designing graphene structures with controlled distributions of topological defects: A case study of toughness enhancement in graphene ruga, Extreme Mech. Lett. **1**, 3 (2014).

[20] R. K. Singh, R. Kumar, and D. P. Singh, Graphene oxide: Strategies for synthesis, reduction and frontier applications, RSC Adv. **6**, 64993 (2016).
[21] R. Wu, Y. Wang, L. Chen, L. Huang, and Y. Chen, Control of the oxidation level of graphene oxide for high efficiency polymer solar cells, RSC Adv. **5**, 49182 (2015).
[22] N. Morimoto, T. Kubo, and Y. Nishina, Tailoring the oxygen content of graphite, and reduced graphene oxide for specific applications, Sci. Rep. **6**, 21715 (2016).
[23] S. J. Stuart, A. B. Tutein, and J. A. Harrison, A reactive potential for hydrocarbons with intermolecular interactions, J. Chem. Phys. **112**, 6472 (2000).
[24] A. P. Thompson *et al.*, LAMMPS - A flexible simulation tool for particle-based materials modeling at the atomic, meso, and continuum scales, Comp. Phys. Comm. **271**, 108171 (2022).
[25] www.lammps.com.
[26] S. A. Svatek, O. R. Scott, J. P. Rivett, K. Wright, M. Baldoni, E. Bichoutskaia, T. Taniguchi, K. Watanabe, A. J. Marsden, N. R. Wilson, and P. H. Beton, Adsorbate-induced curvature and stiffening of graphene, Nano Lett. **15**, 159 (2015).
[27] J. Gu and F. Sansoz, An atomistic simulation study of the mechanisms and kinetics of surface bond strengthening in thermally-treated cone-stacked carbon nanofibers, Carbon **56**, 351 (2013).
[28] S. A. Meguid, A. R. Alian, and M. A. N. Dewapriya, Atomistic modelling of nanoindentation of multilayered graphene-reinforced nanocomposites, in *Micromechanics and Nanomechanics of Composite Solids* (Springer International Publishing, New York, 2017), pp. 39–70, 10.1007/978-3-319-52794-9_2.
[29] I. Giordanelli, M. Mendoza, J. S. Andrade, M. A. F. Gomes, and H. J. Herrmann, Crumpling damaged graphene, Sci. Rep. **6**, 25891 (2016).
[30] Z. Zhang, A. Kutana, A. Roy, and B. I. Yakobson, Nanochimneys: Topology and thermal conductance of 3D nanotube–graphene cone junctions, J. Phys. Chem. C **121**, 1257 (2017).
[31] See Supplemental Material at http://link.aps.org/supplemental/10.1103/PhysRevLett.129.096102 for simulations of large-scale shape control, examples of non-Ising states, and associated input files.
[32] J. Sanchez, F. Ducastelle, and D. Gratias, Generalized cluster description of multicomponent systems, Physica (Amsterdam) **128A**, 334 (1984).
[33] S. Pandit and M. De, Roles of edges and surfaces of graphene oxide in molecular recognition of proteins: Implications for enzymatic inhibition of -chymotrypsin, ACS Appl. Nano Mater. **3**, 3829 (2020).
[34] K. Kenry, K. P. Loh, and C. T. Lim, Molecular interactions of graphene oxide with human blood plasma proteins, Nanoscale **8**, 9425 (2016).
[35] M. Munz, C. E. Giusca, R. L. Myers-Ward, D. K. Gaskill, and O. Kazakova, Thickness-dependent hydrophobicity of epitaxial graphene, ACS Nano **9**, 8401 (2015).
[36] T. Alava, J. A. Mann, C. Théodore, J. J. Benitez, W. R. Dichtel, J. M. Parpia, and H. G. Craighead, Control of the graphene–protein interface is required to preserve adsorbed protein function, Anal. Chem. **85**, 2754 (2013).
[37] J. Feng and Z. Guo, Wettability of graphene: From influencing factors and reversible conversions to potential applications, Nanoscale Horiz. **4**, 339 (2019).
[38] P. Poulin, R. Jalili, W. Neri, F. Nallet, T. Divoux, A. Colin, S. H. Aboutalebi, G. Wallace, and C. Zakri, Superflexibility of graphene oxide, Proc. Natl. Acad. Sci. U.S.A. **113**, 11088 (2016).
[39] S. P. Jordan and V. H. Crespi, Theory of Carbon Nanocones: Mechanical Chiral Inversion of a Micron-Scale Three-Dimensional Object, Phys. Rev. Lett. **93**, 255504 (2004).
[40] Y. Liu and B. I. Yakobson, Cones, pringles, and grain boundary landscapes in graphene topology, Nano Lett. **10**, 2178 (2010).
[41] Y. Wang and V. H. Crespi, Theory of finite-length grain boundaries of controlled misfit angle in two-dimensional materials, Nano Lett. **17**, 5297 (2017).
[42] A. C. T. van Duin, S. Dasgupta, F. Lorant, and W. A. Goddard, ReaxFF: A reactive force field for hydrocarbons, J. Phys. Chem. A **105**, 9396 (2001).
[43] G. te Velde, F. M. Bickelhaupt, E. J. Baerends, C. F. Guerra, S. J. A. van Gisbergen, J. G. Snijders, and T. Ziegler, Chemistry with ADF, J. Comput. Chem. **22**, 931 (2001).
[44] ADF 2019.3, SCM, Theoretical Chemistry, Vrije Universiteit, Amsterdam, The Netherlands, http://www.scm.com (2019).
[45] K. Chenoweth, A. C. T. van Duin, and W. A. Goddard, ReaxFF reactive force field for molecular dynamics simulations of hydrocarbon oxidation, J. Phys. Chem. A **112**, 1040 (2008).
[46] Z. Yang, Y. Sun, F. Ma, Y. Lu, and T. Zhao, Pyrolysis mechanisms of graphene oxide revealed by ReaxFF molecular dynamics simulation, Appl. Surf. Sci. **509**, 145247 (2020).
[47] M. Kowalik, C. Ashraf, B. Damirchi, D. Akbarian, S. Rajabpour, and A. C. T. van Duin, Atomistic scale analysis of the carbonization process for c/h/o/n-based polymers with the ReaxFF reactive force field, J. Phys. Chem. B **123**, 5357 (2019).
[48] S. G. Srinivasan, A. C. T. van Duin, and P. Ganesh, Development of a ReaxFF potential for carbon condensed phases and its application to the thermal fragmentation of a large fullerene, J. Phys. Chem. A **119**, 571 (2015).
[49] C. Ashraf and A. C. van Duin, Extension of the ReaxFF combustion force field toward syngas combustion and initial oxidation kinetics, J. Phys. Chem. A **121**, 1051 (2017).
[50] Private communication from M. Kowalik provided a further optimization of the potential parameters.
[51] J. Liu, D. S. Grierson, N. Moldovan, J. Notbohm, S. Li, P. Jaroenapibal, S. D. O'Connor, A. V. Sumant, N. Neelakantan, J. A. Carlisle, K. T. Turner, and R. W. Carpick, Preventing nanoscale wear of atomic force microscopy tips through the use of monolithic ultrananocrystalline diamond probes, Small **6**, 1140 (2010).
[52] S. Sheng, D. M. Czajkowsky, and Z. Shao, AFM tips: How sharp are they?, J. Microsc. **196**, 1 (1999).
[53] K. Lai, W.-B. Zhang, F. Zhou, F. Zeng, and B.-Y. Tang, Bending rigidity of transition metal dichalcogenide monolayers from first-principles, J. Phys. D **49**, 185301 (2016).

[54] P. E. Lammert and V. H. Crespi, Graphene cones: Classification by fictitious flux and electronic properties, Phys. Rev. B **69**, 035406 (2004).

[55] N. Levy, S. A. Burke, K. L. Meaker, M. Panlasigui, A. Zettl, F. Guinea, A. H. C. Neto, and M. F. Crommie, Strain-induced pseudo-magnetic fields greater than 300 tesla in graphene nanobubbles, Science **329**, 544 (2010).

[56] S. T. Gill, J. H. Hinnefeld, S. Zhu, W. J. Swanson, T. Li, and N. Mason, Mechanical control of graphene on engineered pyramidal strain arrays, ACS Nano **9**, 5799 (2015).

[57] Y. Zhang, M. Heiranian, B. Janicek, Z. Budrikis, S. Zapperi, P. Y. Huang, H. T. Johnson, N. R. Aluru, J. W. Lyding, and N. Mason, Strain modulation of graphene by nanoscale substrate curvatures: A molecular view, Nano Lett. **18**, 2098 (2018).

[58] Y. Zhang, Y. Kim, M. J. Gilbert, and N. Mason, Magneto-transport in a strain superlattice of graphene, Appl. Phys. Lett. **115**, 143508 (2019).

[59] P. Kang, K.-H. Kim, H.-G. Park, and S. Nam, Mechanically reconfigurable architectured graphene for tunable plasmonic resonances, Light **7**, 17 (2018).